



# In Situ Tracking of Break-up, Resuspension, and Transport of Reactive Particle Structures in a Single Wall-Flow Filter Channel

Julia R. D. Thieringer<sup>1</sup> · Heike Werling<sup>1</sup> · Jörg Meyer<sup>1</sup> · Achim Dittler<sup>1</sup>

Received: 24 December 2022 / Revised: 26 December 2022 / Accepted: 16 May 2023  
© The Author(s) 2023

## Abstract

Particulate filters are used as a standard component in the exhaust gas aftertreatment of vehicles. The reactive (soot) and inert (ash) particles generated during engine operation are deposited in wall-flow filter. The resulting particle layer increases the differential pressure of the filter, which is why it is regenerated regularly. During regeneration of the filter, the reactive particles oxidize, and the inert particles remain in the filter. The oxidation of the soot particles results in a layer break-up, and the resuspension of particle structures can occur. The layer break-up over the entire length of an inlet channel and the resuspension of particle structures have not yet been observed, which is why the fundamental processes in a particulate filter have not yet been fully clarified. In these investigations, the regeneration of a single wall-flow filter channel is observed in situ with high temporal and spatial resolution. For this purpose, the filter is loaded with soot particles and regenerated subsequently. The regeneration of the filter is analyzed in relation to the process parameters of temperature, layer thickness, and flow velocity. Before the visual layer break-up, the pressure drop decreases and declines to a constant value before resuspension of particle structures are detected. As the temperature is increased, the regeneration time is reduced. With a thicker particle layer, the particle structures formed during layer break-up become larger, the location of resuspension shifts to the posterior channel region, and the number of resuspensions increases. A higher flow velocity causes more particle structures to be resuspended and transported to the channel end.

**Keywords** Wall-flow filter · Regeneration · Reactive particle layer · Resuspension · Transport · Tracking

## 1 Introduction

Particulate filters have become indispensable in the exhaust gas aftertreatment of vehicles [1]. They reduce emissions generated from the engine combustion and will continue to be used in the future for exhaust gas cleaning of vehicles. Wall-flow filters consist of parallel arranged and alternately closed channels [2, 3]. The exhaust gas aerosol, which is mainly composed of ash and soot particles, flows into the inlet channel, the gas passes through the filter walls and the particles are deposited in and on the porous filter wall [4, 5]. The resulting layer of particles increases the pressure drop and the filtration efficiency of the filter, which influences the operating behavior of the combustion engine [6, 7]. The filter

is therefore regenerated regularly [4, 8]. During regeneration of the filter, the exhaust gas temperature is increased. As a result, soot particles oxidize [9]. This causes the particle layer to break up and individual particle structures can be resuspended and transported.

Sappok et al. (2013) have carried out the first investigations of observing the formation and transport of soot and ash deposits in a diesel particulate filter (DPF) during its regeneration. For this purpose, they installed an optical access to a small section of an external channel of a DPF and observed it with a stereo microscope. Before regeneration, the filter was loaded with soot particles that a closed particle layer was formed. In the process of regeneration, the layer breaks up and particle structures are generated. Shortly after the layer broke up, particle structures were observed to be blown into the small field of the camera's view. In some cases, these structures were subsequently resuspended and transported out of the field of view again, in the direction of the end of the channel. Where the particle structures were resuspended and whether they were transported to the end of the channel

✉ Julia R. D. Thieringer  
julia.thieringer@kit.edu

<sup>1</sup> Karlsruhe Institute of Technology, Institute of Mechanical Process Engineering and Mechanics, Straße am Forum 8, 76131 Karlsruhe, Germany

after resuspension could not be determined by these investigations [10].

For particle structures to be resuspended, the shear force of the gas flow has to exceed the adhesive forces between the particles and the filter medium. Kamp et al. (2014) investigated the attractive interaction forces between soot particles and a DPF surface. The results showed that the interparticle attractive forces between the soot particles are an order of magnitude larger than those between the DPF surface and the soot particles [11]. During the regeneration of the soot particles, these forces decrease, allowing particle structures to resuspend over time. In addition, the particle structures have to be in a resuspendable size range. According to Schmidt and Nitschke (2006) [12], large particles above  $500\mu\text{m}$  only roll or slide on the surface. These particles cannot be resuspended. Smaller particles with a size of about  $10\mu\text{m}$  to  $500\mu\text{m}$  are resuspendable and can be transported if the flow velocity is sufficient. Particle structures smaller than  $10\mu\text{m}$  are not resuspendable [12, 13]. The ranges mentioned have been determined for spherical particles. When a particle layer is broken up during the regeneration process, the particle structures created are mainly in the form of platelets, which is why the ranges for these investigations should be regarded as a guide value.

In the previous investigations on the regeneration of a particulate filter and the resulting layer break-up as well as the resuspension, it could not yet be clarified where the particle structures are resuspended and where they are transported to. Therefore, in these investigations, a complete inlet channel of a wall-flow filter is observed during the regeneration of the filter. The fundamental processes during regeneration (layer break-up, resuspension, transport) of the reactive particle layer are in situ observed over the complete channel length. Additionally, possible resuspensions and their transport can be detected. The observation is carried out with a high temporal and spatial resolution, so that the resulting particle structures can be evaluated in their size as well as tracked in time. For this purpose, a particle layer of reactive particles is generated in the filter channel. Subsequently, the model filter channel is regenerated. The layer break-up, resuspension, and transport are observed and analyzed.

## 2 Materials and Methods

### 2.1 Model Filter Channel

The model filter channel consists of a single inlet and outlet channel of a wall-flow filter. Figure 1 shows a CAD drawing of the constructed channel and its cross sections. The model filter channel consists of three layers. The bottom layer represents the outlet channel. Above is the layer of the inlet channel. The top layer consists of the downholder, which attaches the glass for visual observation and thus closes the model filter channel.

The aerosol (during filtration) or the particle-free air (during observation of the regeneration of the filter) enters the inlet of the model filter channel parallel to the filter medium. The particles are deposited on the sintered metal filter, which is mounted between the inlet and outlet channels. The gas flows through the sintered metal filter and exits the channel through the outlet. The inlet channel is covered at the top by a quartz glass plate. This enables the entire inlet channel to be observed with a high-speed camera (CP90-25PM72, Optronis GmbH, Kehl, Germany). This configuration allows real-time imaging of the regeneration process and thus the observation of soot oxidation as well as the subsequent layer break-up and resuspension of particle structures. The plug and the walls of the filter channel are made of stainless steel. The width of the channel is 3 mm. Due to the sealings, the channel height is 4 mm. The visible area that can be observed with the camera is 125 mm. In the inlet channel is an inlet area of 5 mm before the flow passes through the sintered metal filter. This inlet area is to ensure a stationary flow in the channel with low vortex formation. The difference to a conventional particulate filter is that due to the closed side walls as well as the cover by the quartz glass plate, only one plane is flowed through by the gas. For all experiments, the model filter channel is arranged as shown in Fig. 1, so that the gravitational force acts in the negative Z-direction.

### 2.2 Particle System—Soot Particles

The soot particles are produced with the MiniCAST 6204C soot generator (Jing Ltd., Zollikofen, Switzerland). The principle is based on the incomplete combustion of a propane

**Fig. 1** CAD-image and schematic drawings of the model filter channel

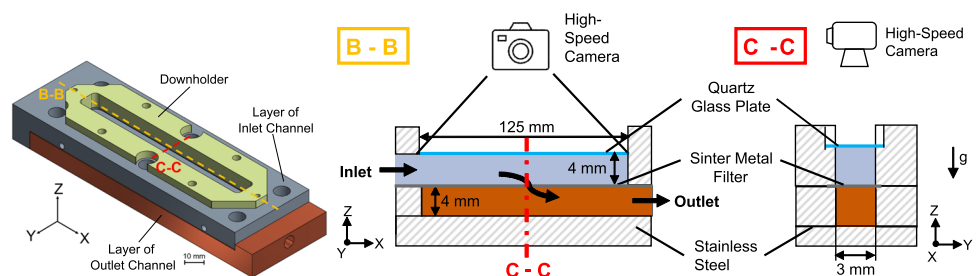


**Table 1** Operating conditions of the soot generator

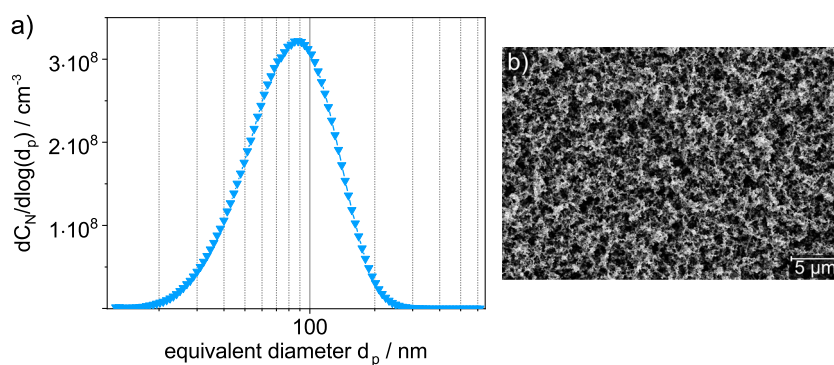
Gas	Flow rate/L min <sup>-1</sup>
Propane	0.05
Quench gas (nitrogen)	2.0
Oxidation air	1.0
Mixing gas (nitrogen)	0.0
Dilution air	0.0

gas flame quenched with nitrogen. The set flow rates for the operating point of the soot generator are listed in Table 1. The operating point remains constant for all experiments, ensuring a constant soot mass flow of 40 mg h<sup>-1</sup> at an exhaust volume flow of 3.05 L min<sup>-1</sup>.

The number-based particle size distribution of the soot particles was measured using a Scanning Mobility Particle Sizing (SMPS) system and is shown in Fig. 2a. The SMPS consists of a Differential Mobility Analyzer (DMA 3082, TSI Incorporated, Shoreview, MN; USA) and a Condensation Particle Counter (CPC 3756, TSI Incorporated, Shoreview, MN, USA). The particle size distribution was measured directly at the outlet of the soot generator with a dilution air flow of 200 L min<sup>-1</sup>.

The number-based particle size distribution of the soot is narrowly distributed. The modal value of the log-normal size distribution is 90 nm. This distribution does not refer to the primary particles of the soot, but to the measured agglomerates formed during incomplete combustion. The formed soot layer is shown in Fig. 2b. The individual primary particles are 20–40 nm in size and accumulate into agglomerates. Due to the use of this selected type of soot, the soot reactivity remains constant during all experiments. The temperature of the maximum conversion rate of soot particles at an oxygen concentration of 21% derived from a TPO (temperature programmed oxidation) measurement is 544 °C. In comparison with other types of soot (flame soot, carbon black, diesel soot), as investigated by Hagen et al. (2021), the propane soot used in this study is of high reactivity against oxidation. The temperature of the maximum conversion rate is in a comparable temperature range to soot from diesel direct injection and gasoline direct injection engines [14].

**Fig. 2** a) Number-based particle-size distribution used for the layer formation in the model filter channel measured with SMPS measurement system and b) SEM image of soot particles



## 2.3 Experimental Setup and Procedure

The experiments carried out can be divided into two subsections: firstly, the filtration/layer formation and, secondly, the regeneration of the model filter channel. The experimental setup of the filtration (#1) and regeneration experiments (#2) and a schematic drawing of the particle layer in each case are shown in Fig. 3. The investigated soot particles are described in Chapter 2.2.

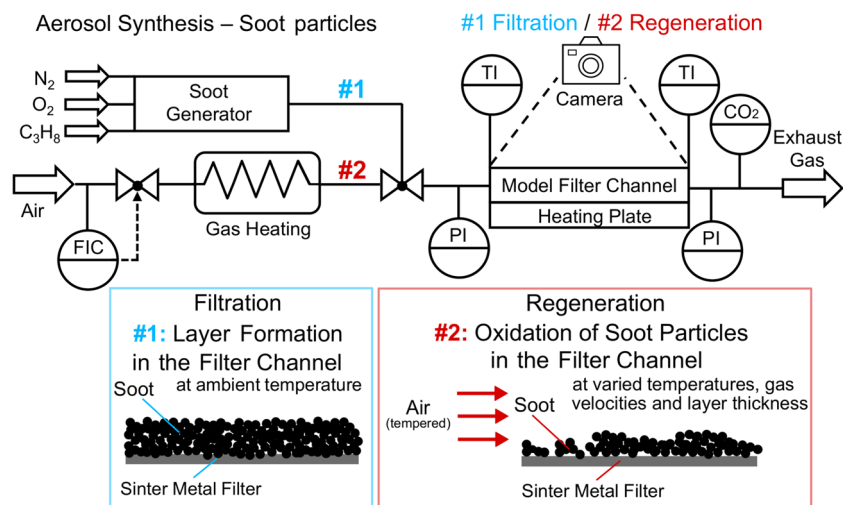
After generation of the soot particles, they are deposited on the sintered metal filter. Meanwhile, the pressure drop across the model filter channel is measured. The loading is mass-based. The average thickness of the soot layer at a loading of 6 mg soot is 68 μm, 12 mg is 135 μm, and 18 mg is 200 μm. The loading takes place at ambient temperature, and the aerosol velocity at the channel inlet is 13.2 ms<sup>-1</sup>.

The process parameters used for the filtration of the soot particles are listed in Table 2.

In the second part of the experiments (#2), the loaded model filter channel is regenerated. The layer break-up as well as the resuspension and transport of particle structures are tracked in time. Particle-free air with an oxygen concentration of 21% is heated with the use of a tube furnace and fed into the model filter channel at a defined flow rate. To reduce heat loss and to ensure that the model filter channel is kept at a sufficient temperature for regeneration, it is additionally heated with a heating plate. At the beginning of the experiment, the model filter channel is at ambient temperature and is heated to 500 °C in the gas phase of the inlet channel within 20 min.

The temperature is measured at the beginning and at the end of the inlet channel. Figure 4 shows the two temperature curves of the temperature measurement at the beginning and end of the inlet channel as well as their temperature difference for a regeneration experiment with an end temperature of 570 °C. The largest temperature differences between channel start and channel end occur in the heating phase of the model filter channel in the first 20 min of the experiment time. After that, the model filter channel reaches an almost constant temperature and the maximum temperature difference between channel beginning and end is 5.5 °C. For this rea-

**Fig. 3** Schematic experimental setup of filtration/layer formation (#1) as well as regeneration experiments (#2) and schematic illustration of the generated reactive particle layer in the model filter channel



son, just the temperature at the beginning of the channel is plotted in the following results of this investigation.

The pressure drop over the filter and the  $CO_2$ -concentration after the filter channel are measured during the regeneration experiments. The layer break-up as well as subsequent resuspensions of particle structures are observed in situ through the top-opened inlet channel with a high-speed camera over the entire channel length. The regeneration experiments were recorded at a minimum frame rate of 100 fps. As soon as the first resuspension was visually observed, the frame rate was changed to 1000 fps in order to observe the transport processes over the channel length. The lower frame rate at the beginning of the experiments was chosen to reduce the amount of data generated. The processes occurring during a regeneration experiment can be divided into two time scales: the process scale and the transport scale. The process scale describes the total regeneration time, which in these studies lasts at least 50 min, depending on the selected process parameters. In comparison, the transport scale lasts only a few milliseconds. This scale describes the transport processes of the resuspended particle structures through the model filter channel. Thus, a high-speed camera with a high temporal as well as spatial resolution is indispensable for these investigations.

The regeneration temperature, flow velocity, and layer thickness were varied for the experiments. Table 3 lists the varied parameter ranges.

The selected velocities as well as regeneration temperatures are in realistic ranges for a regeneration in a particulate

filter ( $T = 450\text{--}600\text{ }^\circ\text{C}$  [4],  $v = 10\text{--}80\text{ ms}^{-1}$  [15]). The specified regeneration temperatures refer to the regeneration end temperature when a constant temperature level has been reached in the filter channel (after the heating phase). During the heating phase of the filter channel ( $T = 20\text{--}500\text{ }^\circ\text{C}$ ), the flow velocity in the inlet channel changes due to the temperature increase, which causes a change in the gas properties. The gas velocities specified refer to the gas velocities at the regeneration end temperature. The gas velocity decreases with the channel length [16, 17].

## 3 Results and Discussion

### 3.1 Regeneration of the Model Filter Channel

Figure 5a shows the temporal development of the layer break-up of a pure soot layer (100% reactive) (a), the temperature curve, the differential pressure over the filter medium, and the  $CO_2$ -concentration (b), which was measured behind the model filter channel over the regeneration time, as well as individual enlarged sections of the filter medium (c) during the experiment at a regeneration end temperature of  $570\text{ }^\circ\text{C}$ , a layer thickness of  $200\text{ }\mu\text{m}$ , and a gas velocity at the channel inlet ( $T = 570\text{ }^\circ\text{C}$ ) of  $60\text{ ms}^{-1}$ . The full-format images of Figure 5c can be found in the supplementary material (Online Resource Fig. 1). The model filter channel is heated during the regeneration experiments from ambient temperature to the regeneration temperature.

**Table 2** Process parameters of filtration/layer formation

Filtration/layer formation	
Particle system	Soot particles
Agglomerate size (modal value)	90 nm
Aerosol velocity (channel inlet, ambient temperature)	$13.2\text{ ms}^{-1}$

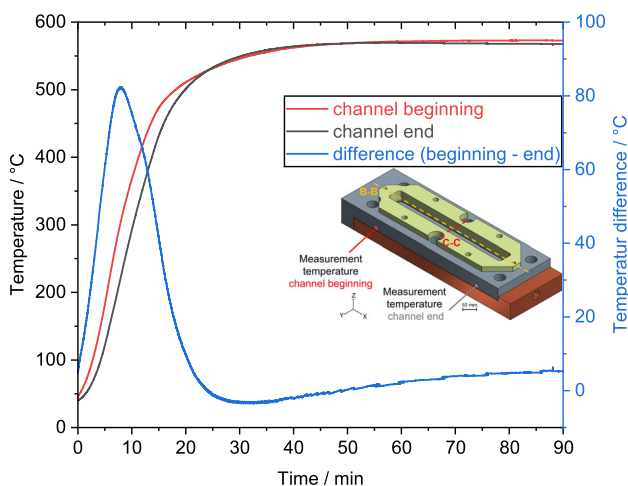


**Fig. 4** Exemplary temperature profiles at the beginning and end of the channel during a regeneration experiment with an end temperature of 570 °C and a soot particle layer. Process parameters:  $T_{\text{end}} = 570^{\circ}\text{C}$ ,  $m_{\text{soot}}(t = 0\text{min}) = 6\text{mg}$  on sinter metal filter (100% reactive), regeneration gas = air (21%  $\text{O}_2$ ),  $v_{\text{end}} = 60\text{ms}^{-1}$

While the temperature in the model filter channel increases, the measured pressure drop and the  $\text{CO}_2$ -concentration remain at approximately constant values. During this time, a uniform black particle layer can be seen (see Fig. 5a). After a regeneration time of 10 min, when a temperature of 291 °C is reached in the model filter channel, the  $\text{CO}_2$ -concentration increases. At this point, the particle layer does not indicate any visual changes and is still present as a black particle layer, but a clear smoke development can be seen (see Fig. 5a). This smoke can be attributed to the high-temperature sealings as well as the high-temperature paste used for the assembly of the model filter channel. Even an empty sintered metal filter produces a  $\text{CO}_2$ -concentration of 972 ppm after 12 min of experimental time and a temperature in the inlet channel of 436 °C during a reference regeneration without particle loading. This confirms that the measured  $\text{CO}_2$ -concentration is not solely caused by the oxidation of the soot. The maximum value of the  $\text{CO}_2$ -concentration could not be detected due to the measurement limit of the  $\text{CO}_2$ -sensor of 2000 ppm. However, at the estimated  $\text{CO}_2$  maximum concentration (time, magnitude), the pressure drop starts to decrease at a temperature of 481 °C after a regeneration time of 19 min. This decrease could be attributed to the start of the regeneration

of the filter, i.e., oxidation of the soot particles. The visual layer break-up can be seen after 22.2 min at a reached temperature in the inlet channel of 517 °C. The oxidation of the soot causes fractures in the particle layer, which increase its permeability and explain the decrease in pressure drop. Other studies on DPFs show comparable results of the course of the pressure drop during the regeneration of a particulate filter, e.g., Choi et al. (2013) [18] and Lapuerta et al. (2012) [19]. After about 30 min regeneration time, the pressure drop (about 40 mbar) as well as the  $\text{CO}_2$ -concentration ( $\approx 585$  ppm) reaches again an almost constant value, which was kept until the end of the experiment. This indicates that the regeneration gas can easily flow through the cracks in the particle layer. The first resuspension takes place after a regeneration time of 30.2 min. The resuspended particle structure has a size of the equal-area circle of 383  $\mu\text{m}$  (see Fig. 5c) and is transported to the end of the channel within 7 ms. The resuspensions of the particle structures have no influence on the pressure drop and do not reduce it further. The experiment was stopped when no more soot was visible on the sinter metal filter (see Fig. 5a).

Figure 6a illustrates the average area of the equivalent diameter for different regeneration times. During the progressing regeneration time, the particle layer breaks-up further that individual particle structures are formed and the filter medium becomes visible.

The resulting particle structures are irregularly shaped and become larger towards the end of the inlet channel. Due to the two-dimensional data evaluation, the analyzed area of the particle structures is converted to an equal-area circle. The average diameter of the equal-area circle increases from 250  $\mu\text{m}$  (first third of channel length) to 442  $\mu\text{m}$  (last third of channel length) after 30 min regeneration time (Fig. 6a). Due to the continuing oxidation of the soot particles, a size reduction of the resulting particle structures takes place (see enlargement Figs. 5c and 6a). The reduction of the area equivalent diameter over the regeneration time decreases with increasing channel length. The average diameter is reduced in the first third of the inlet channel (0–42.6 mm) from 250  $\mu\text{m}$  to 126  $\mu\text{m}$  within 10 min (regeneration time 30–40 min). This corresponds to a size reduction of 49.6%. In the middle and posterior third of the channel length, the size of the particle structures is reduced by 47.1% and 41.6% within 10 min.

**Table 3** Variated process parameters of the regeneration experiments

Variation	Parameter	Values	Constant parameters			
1	Temperature $T_{\text{reg}}/^{\circ}\text{C}$	480	540	570	600	$v_{\text{gas}} = 60\text{ms}^{-1}$ , $h_{\text{layer}} = 68\mu\text{m}$
2	Layer thickness $h_{\text{layer}}/\mu\text{m}$	68	135	200		$T_{\text{reg}} = 570^{\circ}\text{C}$ , $v_{\text{gas}} = 60\text{ms}^{-1}$
3	Gas velocity $v_{\text{gas}}/\text{ms}^{-1}$	10	30	60		$T_{\text{reg}} = 570^{\circ}\text{C}$ , $h_{\text{layer}} = 68\mu\text{m}$

**Fig. 5** a) Time-dependent image sequence of the regeneration experiment of a soot particle layer at 570 °C regeneration end temperature; b) temperature at channel inlet, pressure drop, CO<sub>2</sub>-concentration, and points of the visual layer break-up and resuspension of particulate structures; and c) magnification of an image area of the layer break-up and subsequent size reduction of the reactive particulate structures during the regeneration experiment in the model filter channel. Process parameters:  $T_{\text{end}} = 570^{\circ}\text{C}$ ,  $m_{\text{soot}}(t = 0\text{min}) = 18\text{mg}$  on sinter metal filter (100% reactive), regeneration gas = air (21% O<sub>2</sub>),  $v_{\text{end}} = 60\text{ms}^{-1}$

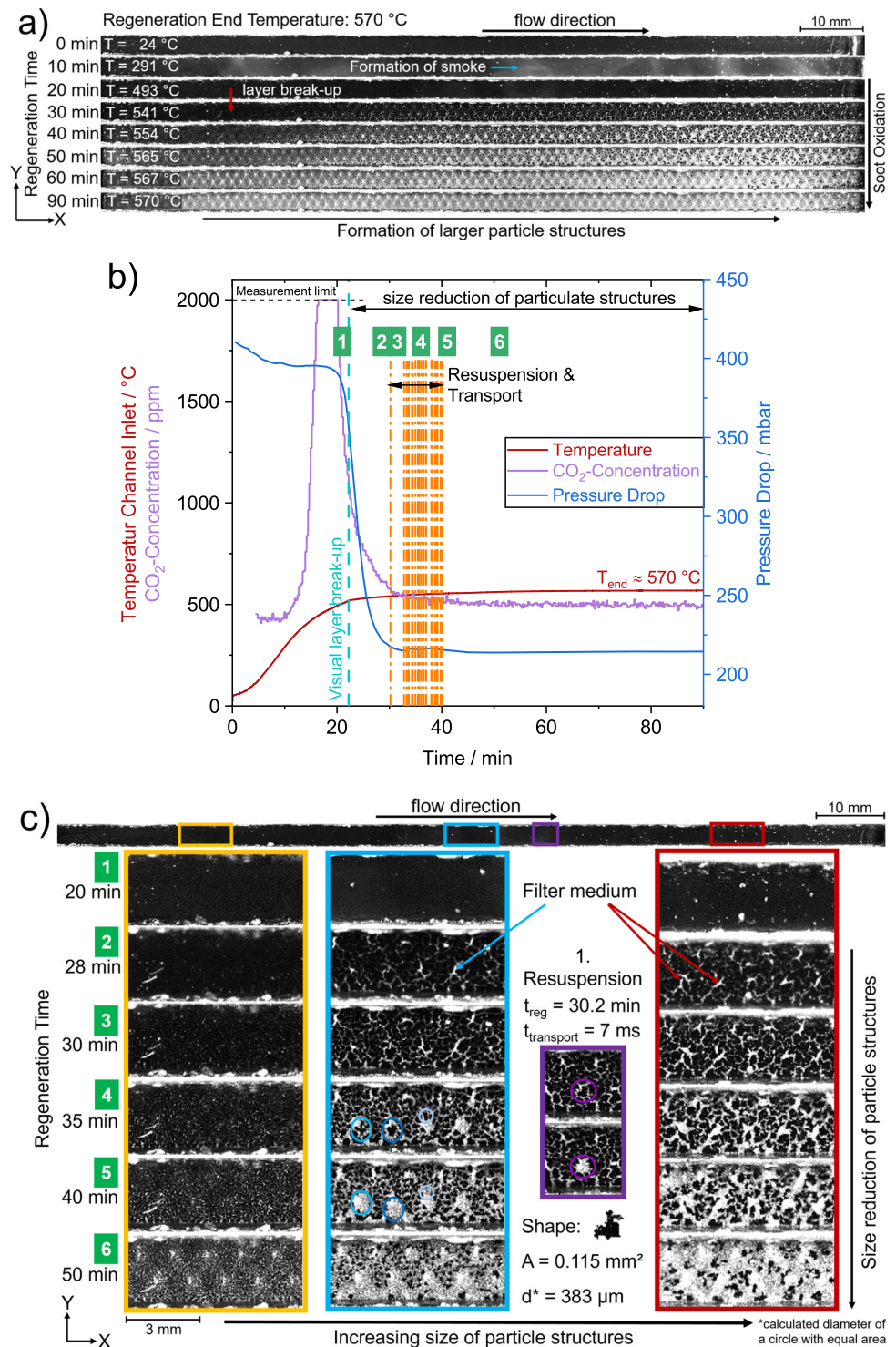
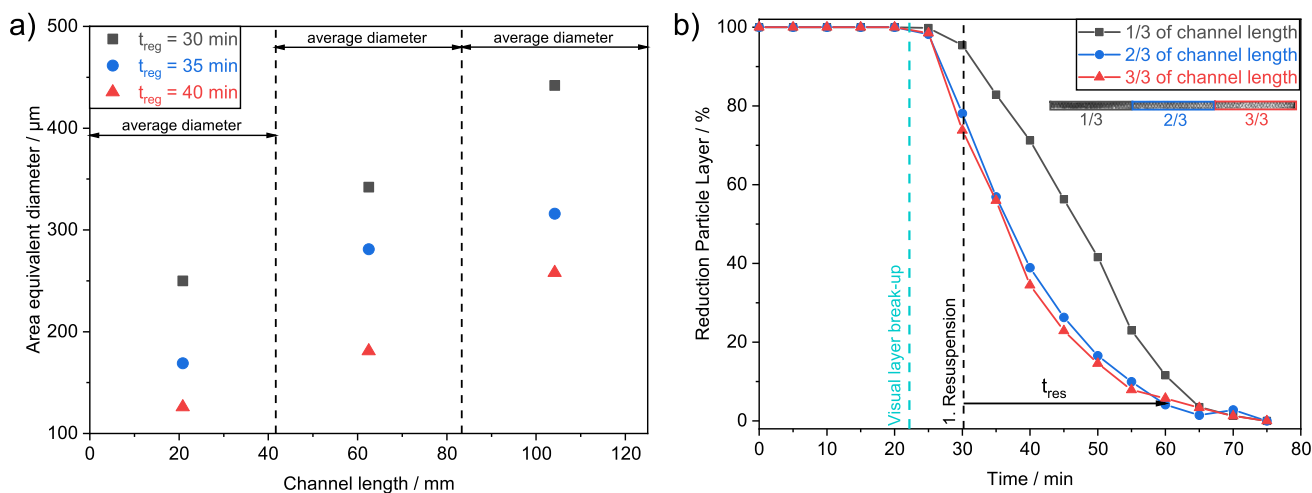


Figure 6b shows the reduction of the particle layer over the regeneration time. The evaluation of the reduction of the particle layer (oxidation of the soot) is performed by analyzing the fraction of black pixels of the captured grayscale image of the high-speed camera. Due to the oxidation of the soot, the proportion of black pixels decreases with time. In

order to evaluate only the influences of regeneration, constant influences such as sealings or shadows of the sealings at the end of the regeneration experiment are subtracted. The reduction of the black pixels as a function of time thus results in the decrease of the loading of the filter medium. The filter is uniformly divided into three ranges (0–41.7 mm; 41.7–



**Fig. 6** a) Average of the area equivalent diameter plotted against channel length for different regeneration times and b) reduction of the particle layer divided into three sections of the channel length during regeneration experiments of a soot particle layer in the model filter

83.3 mm; 83.3–125 mm). After the visual layer break-up, the oxidation of the soot particles and thus the reduction of the particle layer begins in all three areas of the filter channel. The reduction is comparable in the posterior two-thirds (2/3 and 3/3) of the filter. As shown in Fig. 5c, larger particle structures have been formed in this area. From about 51 mm of the channel length and a regeneration time of 30.2 min, particle structures are resuspended and transported along the channel, which will be evaluated in the following. In comparison, the reduction of the particle layer of the first third is slower. This may be due to the thinner layer as well as the smaller particle structures. The smaller particle structures at the beginning of the channel are not resuspended, which means that the reduction of the particle layer is due to the oxidation of the soot.

channel. Process parameters:  $T_{end} = 570^{\circ}\text{C}$ ,  $m_{soot}(t=0 \text{ min}) = 18 \text{ mg}$  on sinter metal filter (100% reactive), regeneration gas = air (21%  $\text{O}_2$ ),  $v_{end} = 60 \text{ ms}^{-1}$

Figure 7a shows the size of the resuspended particle structures plotted against time. The sizes are divided into classes for better clarity. As the regeneration time progresses, the number of smaller particle structures that resuspend increases. This can equally be explained by the continuing oxidation of the soot particles and the associated reduction in size. Large particle structures (400–600  $\mu\text{m}$ ) only dissolve in the first 15 min of the resuspension time.

A total number of 80 particle structures were resuspended and transported along the filter channel during a time of 29.6 min. The number-based particle size distribution of the resuspended structures is shown in Fig. 7b. During the resuspension time, particle structures with a diameter of 110  $\mu\text{m}$  to 553  $\mu\text{m}$  are detached. Thereby, just isolated resuspensions were observed in the classes 150  $\mu\text{m}$  as well as larger than

**Fig. 7** a) Area equivalent diameter plotted against time and b) number-based particle size distribution of the resuspended particle structures during the regeneration of the model filter channel. c) Location of the resuspended particle structures in the model filter channel. Colors indicate the different sizes of the resuspended structures. Process parameters:  $T_{end} = 570^{\circ}\text{C}$ ,  $m_{soot}(t=0 \text{ min}) = 18 \text{ mg}$  on sinter metal filter (100% reactive), regeneration gas = air (21%  $\text{O}_2$ ),  $v_{end} = 60 \text{ ms}^{-1}$

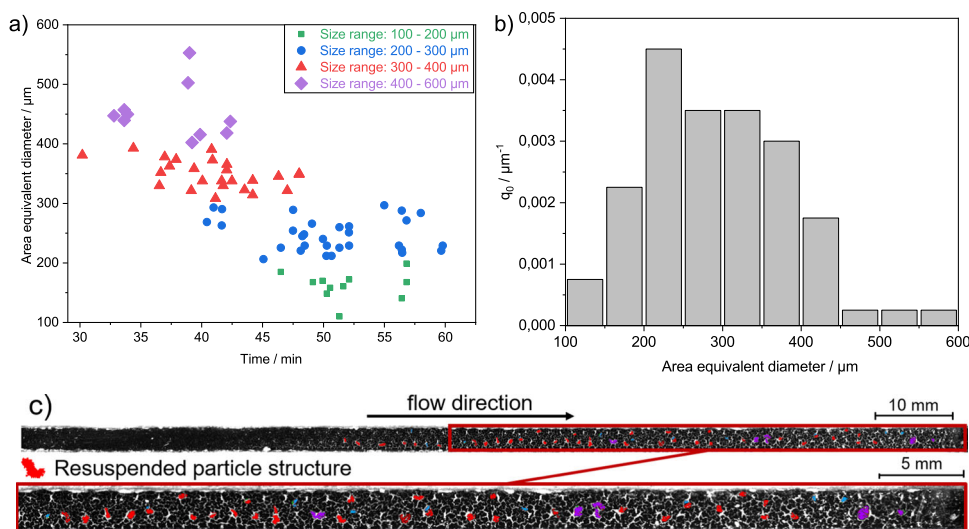
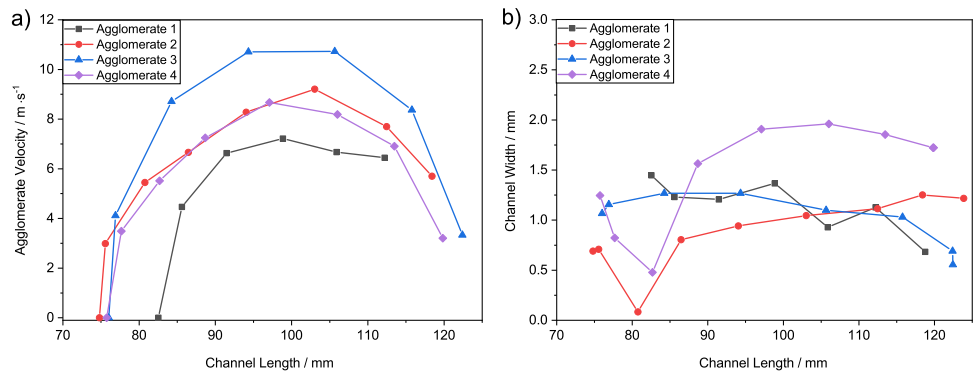


**Fig. 8** a) Agglomerate velocities and b) tracks of resuspended particle structures plotted against the channel length during the regeneration of the model filter channel. Process parameters:  $T_{\text{end}} = 570$  °C,  $m_{\text{soot}}(t=0 \text{ min}) = 18 \text{ mg}$  on sinter metal filter (100% reactive), regeneration gas = air (21%  $\text{O}_2$ ),  $v_{\text{end}} = \text{varied}$



450  $\mu\text{m}$ . Most of the resuspended particle structures are in a size range of 200 - 400  $\mu\text{m}$ . Which is equivalent to 81.25% of the total resuspended particle structures. Particle structures can resuspend when the lift forces overcome the adhesion forces [5, 20]. These forces can be influenced by process parameters such as the flow velocity or the thickness of the particle layer. The size of the evaluated particle structures is also classified as resuspendable in the literature [21]. In these studies, spherical particles are assumed, which is not the case in these investigations. The resuspended particle structures are irregularly shaped and are present as flat platelets. As shown in 7c), the resuspension of the particle structures occurs in the posterior channel region between 51 mm and 121 mm of channel length. The particle structures are mainly detached in the middle of the channel width between 0.5 mm and 2.0 mm. In this area, the core flow of the gas and thus the flow velocity is highest. Near the wall, the structures are resuspended occasionally which is due to the lower flow velocity in this region [5]. The different colors in the figure indicate the different sizes of the resuspended structures. The structure sizes of the fraction between 100  $\mu\text{m}$  and 200  $\mu\text{m}$  (green) cannot be recognized due to their small size. In addition, only half of the resuspension (average of the different size classes) is shown for clarity. No regularity can be recognized in the detachments, since the layer break-up proceeds irregularly and the structures are irregularly shaped. Figure 8 shows the velocity curves (a) and trajectories (b) of four exemplary resuspended agglomerates.

The evaluated agglomerates are resuspended in the second half of the channel, between a channel length of 74.8 mm and 82.5 mm. After resuspension, the agglomerates are accelerated and reach their maximum velocity at a channel length of approx. 100 mm. The maximum velocity reached (between 7.2 and 10.7  $\text{ms}^{-1}$ , see Table 4) differs significantly from the flow velocity at the channel inlet. It has to be noted that the flow velocity of the regeneration gas decreases along the length of the inlet channel. This was simulated in a previous paper by Thieringer et al. [17] for the model filter channel used (two-channel model) using Lattice Boltzmann methods. Other studies by, e.g., Basu et al. (2013) reveal the same results that the velocity in the inlet channels of a DPF decreases with the channel length (DPF specifications: diameter 144 mm, length 152 mm, 200 cpsi, wall thickness 0.38 mm) [22].

Agglomerate 3 has the largest area equivalent diameter of 460  $\mu\text{m}$ . This agglomerate achieves the highest maximum velocity of 10.7  $\text{ms}^{-1}$ . On the one hand, this can be attributed to its larger surface area. On the other hand, the shape of the resuspended particle structure and the height (Z-direction) at which the structure is transported also have an influence on its velocity. No conclusion can be made about the height with the experimental setup used, due to the two-dimensional images. The velocity curves as well as the X-location of the resuspensions of agglomerates 2 and 4 are comparable. The size of these two agglomerates differs by 47  $\mu\text{m}$  for the equal-area circle. This difference can be related to the irregular shapes

**Table 4** Evaluated parameters of the transport of particle structures at a layer thickness of 200  $\mu\text{m}$

	Agglomerate 1	Agglomerate 2	Agglomerate 3	Agglomerate 4
Time resuspension	32.8 min	33.6 min	33.6 min	34.4 min
Duration resuspension	0.006 s	0.008 s	0.007 s	0.008 s
Location X (t = 0 s)	82.5 mm	74.8 mm	76.0 mm	75.4 mm
Location Y (t = 0 s)	1.45 mm	0.69 mm	1.07 mm	1.25 mm
Diameter area equivalent circle	449 $\mu\text{m}$	442 $\mu\text{m}$	460 $\mu\text{m}$	395 $\mu\text{m}$
Maximal velocity	7.2 $\text{ms}^{-1}$	9.2 $\text{ms}^{-1}$	10.7 $\text{ms}^{-1}$	8.7 $\text{ms}^{-1}$

Process parameters:  $T_{\text{end}} = 570$  °C,  $m_{\text{soot}}(t=0 \text{ min}) = 18 \text{ mg}$  on sinter metal filter (100% reactive), regeneration gas = air (21%  $\text{O}_2$ ),  $v_{\text{end}} = 60 \text{ ms}^{-1}$

of the particle structures. Agglomerate 1 reaches the lowest velocity, which can be attributed to the resuspension location, which is further back in the inlet channel.

Figure 8b shows the trajectories of the resuspended particle structures in X- and Y-directions (length and width of the inlet channel). The particle structures detach in the lower half of the channel width (0–1.5 mm). Agglomerates 1 and 3 remain on their trajectory in the center of the channel, where the core flow is located and thus the highest gas velocity is reached. After resuspension, agglomerates 2 and 4 are transported to the lower channel wall (cf. Fig. 8, example agglomerate 2) before moving to the channel midline and being transported to the channel end. The particle structures resuspended in this experiment are transported to the end of the channel and deposited there again.

### 3.2 Influence of Temperature on Filter Regeneration

The influence of the regeneration temperature was investigated with a reactive soot particle layer at four different regeneration temperatures and a layer thickness of 68  $\mu\text{m}$ . The experiments start at ambient temperature. For this reason, a steep temperature rise can be observed in the first 20 min of the experiment, as already explained in Section 2.3.2. Figure 9a shows the temperature curves of the experiments, as well as the pressure drop profiles. The temperature increase of the regeneration gas (particle-free air, 21% oxygen concentration) at the inlet of the model filter channel is constant for all experiments up to a temperature of 480 °C. Subsequently, the final temperature of the experiments (480 °C, 540 °C, 570 °C, and 600 °C) is approached. In the experiment at 480 °C, a slight oscillation can be seen due to the slow control (see Fig. 9a at a regeneration time of 20 min). This may slightly influence the regeneration rate of the soot particles, but the difference to the higher (540–600 °C) temperatures is large that this overshoot is not considered in more detail here. Due to the different end temperatures and the resulting change in gas properties, the final velocity of the gas in the channel varies between 55  $\text{ms}^{-1}$  and 60  $\text{ms}^{-1}$ . According to current knowledge, this difference has no influence on possible rearrangements, but it does lead to a small difference in the pressure drop across the model filter channel.

During the heating phase of the model filter channel, the pressure drop decreases slightly (up to approx. 12 min), which is due to the desorption of volatile components. A TGA (thermogravimetric analysis) of the propane soot indicated that from a temperature of 70 °C, the first components had already desorbed. During this time, no CO or CO<sub>2</sub> is generated. In conclusion, no oxidation of the soot occurs at the investigated temperatures in the heating phase. At a temperature at the channel inlet of 480 °C, the pressure drop starts to decrease in all experiments. After this decrease, the visual layer breakup is also visible by visual observation with

the camera. The layer break-up occurs between 14.7 min and 21.5 min (see Table 5). This break-up of the particle layer, due to the oxidation of the soot particles, causes the pressure drop to decrease. After about 40 min of the experiment, this remains at a constant value at the temperatures investigated. Table 5 lists the parameters of the regeneration time, the duration of the steep pressure drop, the time of the visual layer breakup, the first resuspension, their duration, and their number.

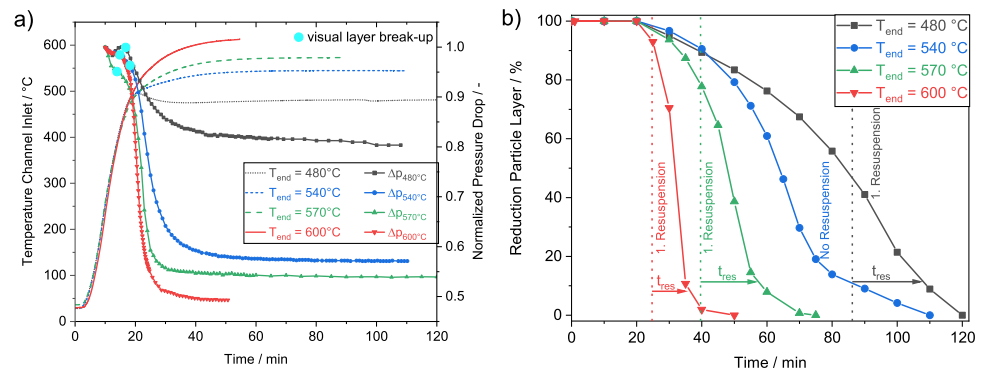
Increasing the regeneration temperature reduces the regeneration time. At a regeneration end temperature of 480 °C, the filter medium is not completely removed from the soot even after 2 h of regeneration time. At a temperature of 600 °C, the particles are completely oxidized after 51 min. This corresponds to a reduction of the regeneration time of 55%. The increased temperature causes the conversion rate of soot oxidation to rise. The increased oxidation rate of soot can also be seen in the faster reduction of the pressure drop, which is reduced from 54 min at 480 °C to 10 min at 600 °C.

Fig. 9b) shows the reduction of the particle layer during the experimental time for the investigated regeneration temperatures. With increasing regeneration temperature, the particle layer is reduced faster, and the resuspension of particle structures occurs earlier. After the beginning of resuspension of particle structures, the coverage of the particle layer decreases more rapidly in all experiments. In this region, two processes coincide. One is the oxidation of the soot particles and the associated size reduction of the particle structures, and the other is their resuspension. These two parallel processes can result in an increased reduction of the particle layer. The sharpest reduction in the particle layer is at a regeneration temperature of 600 °C and decreases as the temperature is reduced.

In relation to the reduction of the particle layer and the shorter regeneration time, the resuspension time of particle structures decreases with increasing temperature. Due to the higher temperature, the particle structures reach a resuspendable size more quickly. Resuspension of particle structures occurs at all temperatures up to a reduction of the soot layer of about 10%. In this range, individual particle structures are present on the filter medium, which on the one hand are of a size that cannot be resuspended and on the other hand are frequently present in the second half of the inlet channel. In this area, the flow velocity of the regeneration gas is significantly reduced, with the result that no more particle structures are resuspended.

At a regeneration temperature of 540 °C, no resuspensions can be detected. Due to the small particle structures as well as a worse contrast of the video recordings in this experiment, possible resuspensions could not be tracked and therefore not be evaluated. With the trends of the three other temperatures as well as the reduction of the layer break-up, resuspensions should also occur in this case. The decrease of the soot layer

**Fig. 9** a) Temperature profile at the channel inlet as well as normalized pressure drop and b) the reduction of the particle layer during regeneration experiments of a soot particle layer at different regeneration end temperatures in the model filter channel. Process parameters:  $T_{\text{end}} = \text{varied}$ ,  $m_{\text{soot}}(t=0 \text{ min}) = 6 \text{ mg}$  on sinter metal filter (100% reactive), regeneration gas = air (21%  $\text{O}_2$ ),  $v_{\text{end}} = 60 \text{ ms}^{-1}$



on the sintered metal filter is shown in Figure 10 for a visual comparison. The full format images of Figure 10 can be found in the supplementary material (Online Resource Fig. 2).

It can be seen that the higher the regeneration temperature, the faster the soot particles oxidize and the faster the filter is cleaned. The size of the particle structures is not evaluated accurately due to their small size. Likewise, the resuspensions cannot be tracked and are therefore not evaluated in this section. The results show that with an increase in regeneration temperature from 480 °C to 600 °C, the regeneration time is reduced by 55% in the system studied. However, it should be noted that the regeneration temperature of 600 °C is at the upper limit of temperatures reached in a particulate filter during regeneration [4, 23]. For this reason, a regeneration end temperature of 570 °C was selected for the following experiments and kept constant for the remaining investigations.

### 3.3 Influence of Layer Thickness on Filter Regeneration

For the investigation of the influence of the layer thickness on the filter regeneration, different soot masses were deposited on the sinter metal filter, thus producing different layer thicknesses.

Figure 11 shows the layer thicknesses after filtration along the length of the channel. The measurements were carried out at three positions on the loaded sintered metal filter.

Differences in the generated layer thicknesses over the channel length can be seen for the particle layers formed. For a loading of 6 mg, the layer thickness decreases by 25.7% towards the end of the channel. With a film thickness of 12 mg by 15.1%, the differences may be due to the time dependence of the flow through the filter medium. The flow velocity of the gas decreases over the channel length. At the beginning of filtration, the gas mainly passes through the filter medium at the beginning of the channel, that particles are increasingly deposited in this area. Due to the particle buildup in this region and the resulting cake filtration, the gas passes through the filter medium further back in the inlet channel. As a result, a homogeneous particle layer is built up in the model filter channel with progressive regeneration time. At the thickest particle layer of 18 mg, the layer thickness is more homogeneously distributed. At the beginning of the channel, the generated particle layer is slightly thinner than in the posterior channel regions. In this case, the deviation between the beginning and end of the channel is 11.6%. This resulted in average thicknesses of the soot particle layer of 68  $\mu\text{m}$  ( $m = 6 \text{ mg}$ ), 135  $\mu\text{m}$  ( $m = 12 \text{ mg}$ ), and 200  $\mu\text{m}$  ( $m = 18 \text{ mg}$ ). In the following evaluations, the average values are used for the three layer thicknesses.

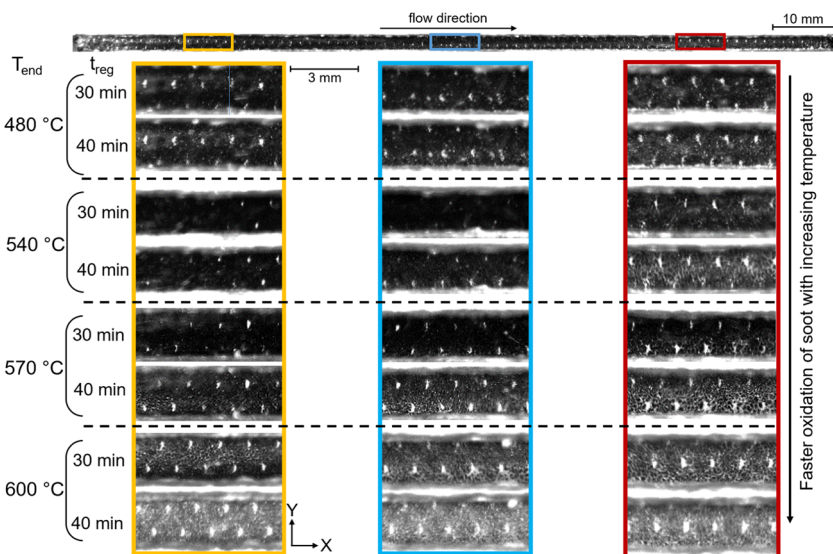
Figure 12 depicts the results of the measured differential pressure across the filter, the temperature profile in the inlet channel (a), and the reduction of the particle layer (b) during regeneration of the model filter channel at a regeneration end

**Table 5** Evaluated parameters of the regeneration experiments at varied regeneration temperatures

Regeneration end temperature	480 °C	540 °C	570 °C	600 °C
Regeneration time	120 min	114 min	76 min	71 min
Duration of decreasing pressure drop	54 min	28 min	20 min	10 min
Visual layer break-up	15.1 min	21.5 min	19.1 min	14.7 min
1. Resuspension	86 min	–	39.5 min	24.8 min
Resuspension time	21 min	–	17 min	10 min
Number of resuspensions	11	–	41	79

Process parameters:  $T_{\text{end}} = \text{varied}$ ,  $m_{\text{soot}}(t=0 \text{ min}) = 6 \text{ mg}$  on sinter metal filter (100% reactive), regeneration gas = air (21%  $\text{O}_2$ ),  $v_{\text{end}} = 60 \text{ ms}^{-1}$

**Fig. 10** Visual observation of the influence of regeneration temperature on the oxidation of the soot particles. Process parameters:  $T_{end}$  = varied,  $m_{soot}(t=0 \text{ min}) = 6 \text{ mg}$  on sinter metal filter (100% reactive), regeneration gas = air (21%  $O_2$ ),  $v_{end} = 60 \text{ ms}^{-1}$



temperature of 570 °C and a gas velocity of 60 ms<sup>-1</sup>. The corresponding values are listed in Table 6.

The measured pressure drop of the three layer thicknesses investigated is comparable. However, a difference can be seen at the beginning of the regeneration. During the heating phase of the channel, the pressure drop of the thickest soot layer is higher and remains constant at one value until it decreases rapidly within 12 min. This may be due to the start of the oxidation of the soot particles. This causes the particle layer to break up and the pressure drop to decrease. Due to the thickness of the layer, this breakup is not yet visually apparent, which is why it occurs later compared to the other layer thicknesses. The thinner particle layers (68 μm and 135 μm) have a lower pressure drop after the start of regeneration,

which decreases gradually after 15 min of regeneration time than in the comparative experiment with the thicker layer (200 μm). The final pressure drop achieved is similar for the three layer thicknesses.

The duration of regeneration is comparable for the layers with a thickness of 68 μm and 135 μm. The regeneration of the thickest layer (200 μm) takes 80 min and is slightly longer than for the thinner layers. This indicates that the oxidation of the soot and thus the regeneration of the filter is mainly temperature-dependent (see also Chapter 3.2). The thickness of the particle layer has a minor influence on the regeneration time, which is also confirmed by the evaluation of the reduction of the particle layer. This is comparable for all three layer thicknesses. The layer break-up occurs at a later stage with increasing layer thickness (see Table 6). Figure 13 shows the comparison of the three fragmented layers of the three different thicknesses after 30 min and 40 min of regeneration time and at three positions in the model filter channel. The full-format images of Figure 13 can be found in the supplementary material (Online Resource Fig. 3).

After a time of 30 min, all layers have broken up (cf. Table 6). In the thinnest layer (68 μm), the small particle structures are formed. The particle structures in the two thicker layers (135 μm and 200 μm), on the other hand, are larger. The break-up behavior and the resulting particle structures also differ within the filter length. As already evaluated in Chapter 3.1, the size of the particle structures increases with the channel length for a layer thickness of 200 μm. For the two thinner particle layers, an opposite behavior can be seen. In this case, the structure sizes decrease with the channel length. Thus, the average size of the particle structures is reduced from 229 μm at the beginning of the channel to 130 μm at the end of the channel for the thinnest layer (68 μm) and from 281 μm to 162 μm for a layer thickness of 135

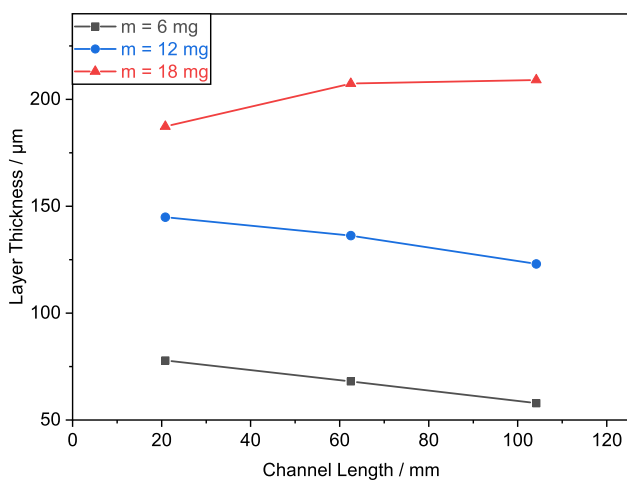
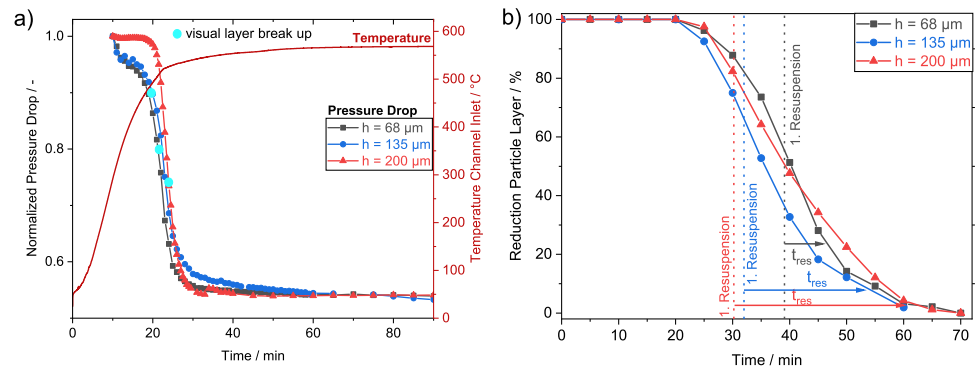


**Fig. 11** Layer thicknesses after filtration of the soot particles with varied masses. Measurement at three points of the filter. Lines between datapoints serve as a guide to the eye. Process parameters:  $T_{end} = 570 \text{ °C}$ ,  $m_{soot}(t=0 \text{ min}) = \text{varied}$  on sinter metal filter (100% reactive), regeneration gas = air (21%  $O_2$ ),  $v_{end} = 60 \text{ ms}^{-1}$

**Fig. 12** a) Temperature profile at the channel inlet as well as normalized pressure drop over the model filter channel and b) reduction of the particle layer during regeneration experiments of a soot particle layer at different layer thicknesses. Process parameters:  $T_{\text{end}} = 570$  °C,  $m_{\text{soot}}(t=0 \text{ min}) =$  varied on sinter metal filter (100% reactive), regeneration gas = air (21%  $\text{O}_2$ ),  $v_{\text{end}} = 60 \text{ ms}^{-1}$



$\mu\text{m}$ . The different sizes of the resulting particle structures could be attributed to the slight variations in film thickness during filtration. As shown in Fig. 11, for the layers with a thickness of  $68 \mu\text{m}$  and  $135 \mu\text{m}$ , the height of the particle layer decreases slightly. The opposite behavior is the case for the particle layer with a thickness of  $200 \mu\text{m}$ .

With increasing layer thickness, the resuspension of particle structures starts earlier. The time in which resuspensions are detected (see Fig. 12b and Table 6) and the number of resuspensions increases. The number-based particle size distribution (a), the time-dependent resuspension of the particle structures (b), and their visual evaluation (c) are depicted in Fig. 14.

As the thickness of the particle layer increases, the number-based particle size distribution of resuspended particle structures becomes wider, which is due to the different break-up behavior and the resulting structure sizes. At a layer thickness of  $68 \mu\text{m}$ , the number-based particle size distribution is narrowly distributed, which is due to the small particle structures formed during layer break-up. The resuspended particle structures are in a size range of the equivalent diameter from  $92 \mu\text{m}$  to  $243 \mu\text{m}$ . The number-based particle size distribution at the medium layer thickness is more widely distributed and particle structures up to  $372 \mu\text{m}$  in diameter are resuspended. For the thickest particle layer, sizes up to  $553 \mu\text{m}$  are detached. The resuspension location also differs for the three layer thicknesses (Fig. 14b). With a layer thickness of  $68 \mu\text{m}$ , resuspension of the particle structures occurs

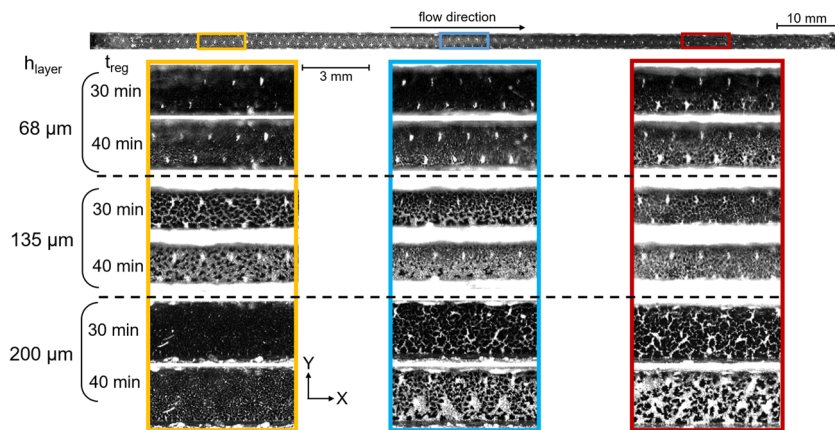
in the front region of the inlet channel (0–20 mm). Due to the small particle structures, larger shear forces are required for their resuspension, which is why they are mainly detached in this region (higher gas velocity). With an increase in layer thickness, the resuspension location of the particle structures shifts along the inlet channel, and the resuspension of particle structures occurs over a longer period of time (see Table 6). From the thinnest to the thickest particle layer, the resuspension period increases by 140%. The resuspension area (area where particle structures detach) of the layer thickness of  $135 \mu\text{m}$  is between 16 mm and 80 mm and for the layer thickness of  $200 \mu\text{m}$  between 51 mm and 121 mm. The differences of the resuspension location is due to the different sizes of the particle structures. Small particle structures ( $< 200 \mu\text{m}$ ) require larger shear forces to be resuspended. For larger structures, as seen at the  $200 \mu\text{m}$  layer thickness, the structures may partially detach from the filter media during oxidation of the soot. Oxidation of the soot structures and the associated size reduction begins at their edges, since this is where the oxygen supply is highest due to the flow through the filter. This allows the structures at the edge to detach while they are still in contact with the filter medium in the center of the structure. Thus, the adhesive forces between the filter medium and the particle layer are reduced. As a result, lower lift forces and consequently a lower gas velocity are required to resuspend the particle structures from the filter medium. This could explain the resuspension of particle structures in the posterior part of the inlet channel. The locations of the

**Table 6** Evaluated parameters of the regeneration experiments at varied layer thicknesses

Layer thickness	$68 \mu\text{m}$	$135 \mu\text{m}$	$200 \mu\text{m}$
Regeneration time	76 min	75 min	80 min
Duration of decreasing pressure drop	20 min	20 min	12 min
Visual layer break-up	19.1 min	21.5 min	25.4 min
1. Resuspension	39.1 min	32.0 min	30.2 min
Resuspension time	16.7 min	30.0 min	40.0 min
Number of resuspensions	41	59	80

Process parameters:  $T_{\text{end}} = 570$  °C,  $m_{\text{soot}}(t=0 \text{ min}) =$  varied on sinter metal filter (100% reactive), regeneration gas = air (21%  $\text{O}_2$ ),  $v_{\text{end}} = 60 \text{ ms}^{-1}$

**Fig. 13** Visual observation of the influence of layer thickness on the oxidation of the soot particles. Process parameters:  $T_{\text{end}} = 570\text{ }^{\circ}\text{C}$ ,  $m_{\text{soot}}(t = 0\text{ min}) = \text{varied}$  on sinter metal filter (100% reactive), regeneration gas = air (21%  $\text{O}_2$ ),  $v_{\text{end}} = 60\text{ ms}^{-1}$



resuspended particle structures are shown in red in Fig. 14c). It can be seen that for all three layer thicknesses, the particle structures are resuspended in the middle of the channel width. This is attributable to the higher velocity in this area again. In the proximity of the wall, only a few structures are resuspended.

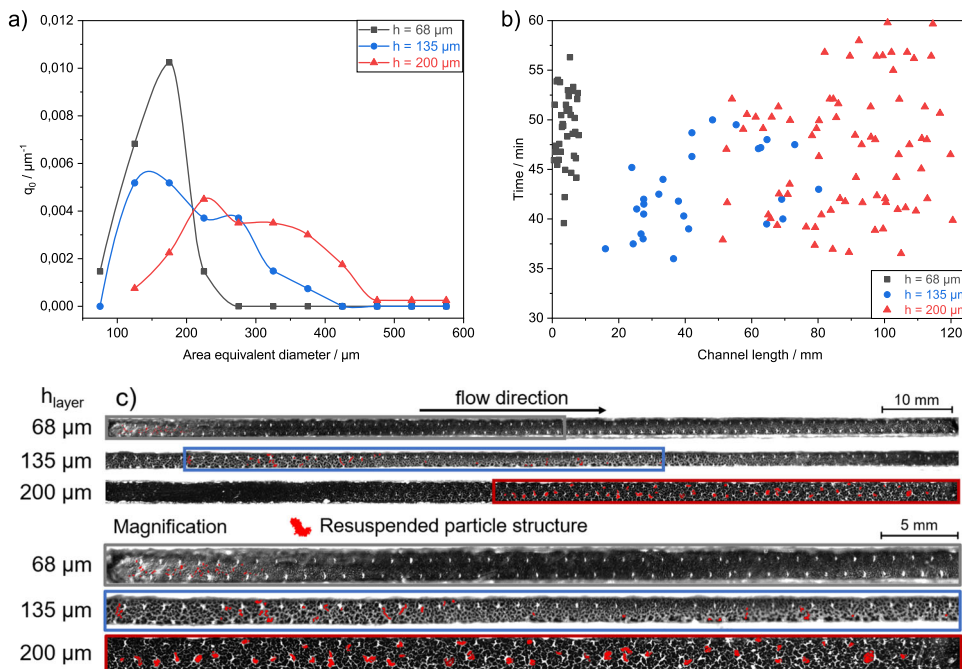
### 3.4 Influence of Gas Velocity on Filter Regeneration

Figure 15 shows the pressure drop across the model filter channel at different flow velocities (10  $\text{ms}^{-1}$ , 30  $\text{ms}^{-1}$ , 60  $\text{ms}^{-1}$ ) of the regeneration gas at the channel inlet. The other process parameters are constant at 570  $^{\circ}\text{C}$  regeneration end temperature and a layer thickness of 68  $\mu\text{m}$ . The gas velocity decreases with the channel length, which was simulated for the model filter channel used by Lattice Boltzmann method

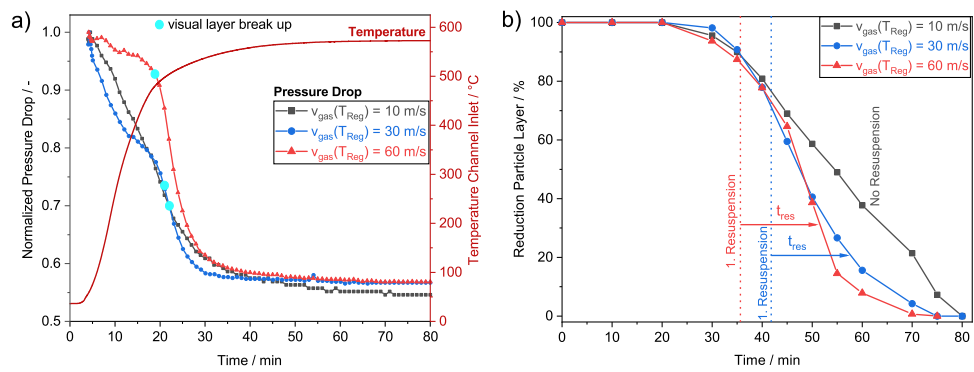
[17]. The heating period is identical for all experiments, which means that the flow velocity increases identically until the end temperature is reached.

At the gas velocities of 10  $\text{ms}^{-1}$  and 30  $\text{ms}^{-1}$ , the pressure drop decreases rapidly from the beginning of the regeneration. In comparison, at a velocity of 60  $\text{ms}^{-1}$ , there is a gentle reduction of the pressure drop at the beginning. In this case, volatile components are desorbed during the heating phase, which influence the particle layer and can cause a reduction in the pressure drop. Shortly before the visual layer break-up after 19.2 min at the largest velocity, the pressure drop starts to fall rapidly at a temperature of 480  $^{\circ}\text{C}$  in the channel inlet. At the lower velocities, the visual layer break-up occurs a bit later after 20.9 min ( $v = 30\text{ ms}^{-1}$ ) as well as 23.3 min ( $v = 10\text{ ms}^{-1}$ ) (see Table 7). The different flow velocities during regeneration have a minor influence on the time of layer

**Fig. 14** a) Number-based particle size distribution and b) time dependence of the resuspended particle structures over the channel length at different thicknesses. c) Visual evaluation of the resuspension location of the particle structures. Process parameters:  $T_{\text{end}} = 570\text{ }^{\circ}\text{C}$ ,  $m_{\text{soot}}(t = 0\text{ min}) = \text{varied}$  on sinter metal filter (100% reactive), regeneration gas = air (21%  $\text{O}_2$ ),  $v_{\text{end}} = 60\text{ ms}^{-1}$



**Fig. 15** a) Normalized pressure drop over the model filter channel as well as temperature profile at the channel inlet and b) reduction of the particle layer during regeneration experiments of a soot particle layer at different inlet gas velocities in the model filter channel. Process parameters:  $T_{\text{end}} = 570\text{ }^{\circ}\text{C}$ ,  $m_{\text{soot}}(t=0\text{ min}) = 6\text{ mg}$  on sinter metal filter (100% reactive), regeneration gas = air (21%  $\text{O}_2$ ),  $v_{\text{end}} = \text{varied}$



break-up. The end pressure drop is reached after a regeneration time of about 40 min and is comparable for the three velocities.

The reduction of the particle layer starts after 20 min (Fig. 15b) and is almost identical up to a regeneration time of 40 min for the three investigated flow velocities. As soon as resuspension starts at the flow velocities of  $30\text{ ms}^{-1}$  and  $60\text{ ms}^{-1}$ , the reduction of the particle layer is significantly faster. At a flow velocity of  $10\text{ ms}^{-1}$ , no resuspension was tracked. The low flow velocity is not sufficient to resuspend the particle structures. In this case, the velocity of the gas and thus the force of the shear stress is not high enough to overcome the adhesive forces between the particle structures and the filter medium. The average diameter of the particle structures in the first third of the channel length is  $201\text{ }\mu\text{m}$  after 40 min of regeneration time. According to current results (see Chapter 3.1), these sizes of particle structures could be resuspended in the model system. A gas velocity of  $10\text{ ms}^{-1}$  is not sufficient to resuspend particle structures in the model system. The sizes of the particle structures in the posterior sections could not be evaluated due to their size and are not discussed further here.

At the flow velocity of  $30\text{ ms}^{-1}$  at the channel inlet, resuspensions are detected after 46.5 min of regeneration time, and a total number of 13 particle structures are detached. Resuspension of particle structures at a flow velocity of  $60\text{ ms}^{-1}$  starts after 39.5 min of regeneration time and 41 particle structures are detached during the regeneration of the filter. The higher gas velocity results in greater shear stress whereby

more structures are resuspended. Figure 16 shows a comparison of the layer breakup after 30 min and 40 min regeneration time for the three gas velocities. The full-format images of Figure 16 can be found in the supplementary material (Online Resource Fig. 4). At all three velocities, the particle layer breaks-up and small particle structures are formed. At the flow velocities of  $10\text{ ms}^{-1}$  and  $30\text{ ms}^{-1}$  velocities, the size of the structure decreases as the channel length increases. The decrease in structure size at the lower gas velocities could be attributed to the regeneration gas flowing through the filter media mainly in the front region of the inlet channel. As the channel length increases, the gas velocity decreases [16] that the regeneration gas at the end of the channel has a velocity that is too low for a visible break-up of the particle layer to occur.

The average size of the particle structures in the first third of the inlet channel differs slightly at the three velocities investigated. At a gas velocity of  $10\text{ ms}^{-1}$ , the average structure size is  $205\text{ }\mu\text{m}$ , at  $30\text{ ms}^{-1}$   $289\text{ }\mu\text{m}$ , and at  $60\text{ ms}^{-1}$   $229\text{ }\mu\text{m}$ . At the gas velocity of  $60\text{ ms}^{-1}$ , the break-up is more uniform. In the posterior region of the inlet channel, the particle structures are slightly larger.

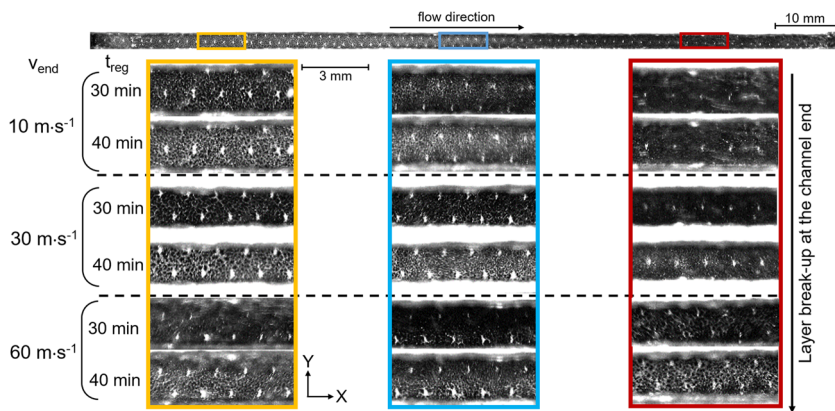
Figure 17 shows the number-based particle size distribution (a), the time-dependent resuspension of the particle structures in relation to the channel length (b), and their visual evaluation (c). The evaluation is carried out for the two velocities of  $30\text{ ms}^{-1}$  and  $60\text{ ms}^{-1}$ , since resuspension of particle structures was observed solely at these velocities.

**Table 7** Evaluated parameters of the regeneration experiments at varied regeneration gas velocities

Velocity	$10\text{ ms}^{-1}$	$30\text{ ms}^{-1}$	$60\text{ ms}^{-1}$
Regeneration time	75 min	67 min	76 min
Duration of decreasing pressure drop	37 min	21 min	20 min
Visual layer break-up	23.3 min	20.9 min	19.2 min
1. Resuspension	–	46.5 min	39.6 min
Resuspension time	–	16.8 min	16.8 min
Number of resuspensions	0	13	41

Process parameters:  $T_{\text{end}} = 570\text{ }^{\circ}\text{C}$ ,  $m_{\text{soot}}(t=0\text{ min}) = 6\text{ mg}$  on sinter metal filter (100% reactive), regeneration gas = air (21%  $\text{O}_2$ ),  $v_{\text{end}} = \text{varied}$

**Fig. 16** Visual observation of the influence of gas velocity on the oxidation of the soot particles. Process parameters:  $T_{\text{end}} = 570\text{ }^{\circ}\text{C}$ ,  $m_{\text{soot}}(t=0\text{ min}) = 6\text{ mg}$  on sinter metal filter (100% reactive), regeneration gas is air (21%  $\text{O}_2$ ),  $v_{\text{end}}$  = varied



The number-based particle size distribution indicates that significantly smaller particle structures are resuspended at the velocity of  $60\text{ ms}^{-1}$ . The distribution at a velocity of  $30\text{ ms}^{-1}$  is wider, and structure sizes between  $139$  and  $394\text{ }\mu\text{m}$  are resuspended. The locations where the structures are detached in the inlet channel, as well as the timing of the resuspensions, are distributed at this velocity as well. At the gas velocity of  $60\text{ ms}^{-1}$ , the particle structures are resuspended in the first half of the channel length and in the middle of the channel width. This is where the gas velocity is at its highest, which enhances the probability of the resuspension of particle structures.

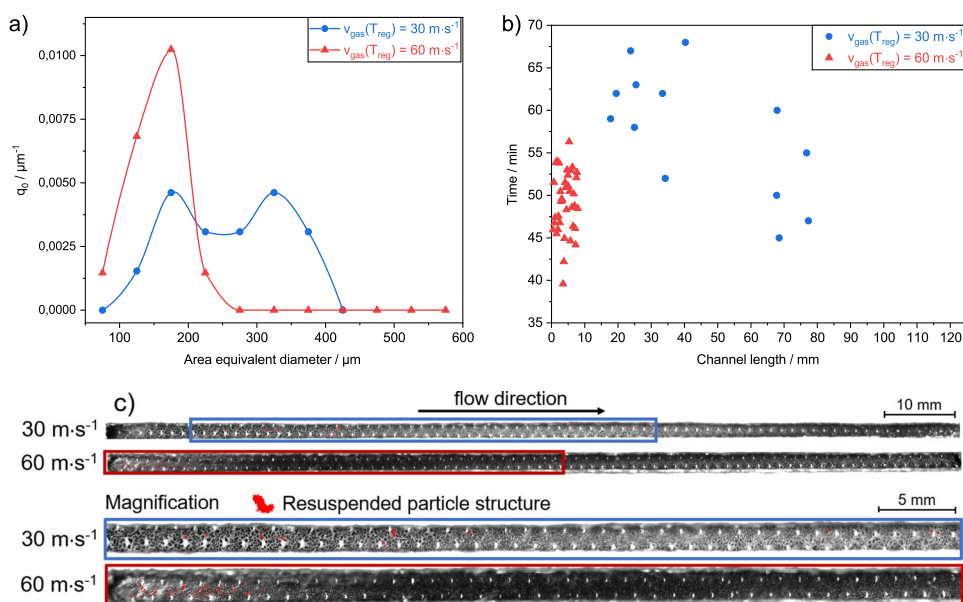
### 4 Conclusion

The processes during the regeneration of a wall-flow filter are not yet completely understood. In situ observation with a high temporal and spatial resolution in a particulate filter dur-

ing the operation of a vehicle is difficult to implement due to the closed system. For this reason, a model filter channel consisting of a single inlet and outlet channel of a wall-flow filter is used in these investigations. Thus, the complete regeneration of the filter with the layer break-up, resuspension, and transport of particle structures is observed. First, a particle layer of soot particles was formed. Subsequently, the model filter was regenerated that the reactive particles oxidize. During this process, the entire inlet channel was observed in situ with a high-speed camera allowing the tracking of the layer break-up as well as the resuspension and transport of particle structures.

As oxidation of the soot particles begins, the pressure drop across the filter decreases and the  $\text{CO}_2$ -concentration reaches its maximum. The visual layer break-up can be seen a few minutes after the decrease in pressure drop. Due to the layer break-up, irregularly shaped particle structures are formed which, for a layer thickness at the beginning of the regeneration of  $200\text{ }\mu\text{m}$ , become larger with the channel length.

**Fig. 17** a) Number-based particle size distribution and b) time dependence of the resuspended particle structures over the channel length at different gas velocities. c) Visual evaluation of the resuspension location of the particle structures. Process parameters:  $T_{\text{end}} = 570\text{ }^{\circ}\text{C}$ ,  $m_{\text{soot}}(t=0\text{ min}) = 6\text{ mg}$  on sinter metal filter (100% reactive), regeneration gas is air (21%  $\text{O}_2$ ),  $v_{\text{end}}$  = varied



During the regeneration period, the size of the particle structures is reduced due to the progressing soot oxidation. After a constant pressure drop is reached, particle structures can be resuspended depending on the regeneration temperature, flow velocity of the regeneration gas, and the layer thickness. At a layer thickness of 200  $\mu\text{m}$ , 81.25% of the resuspended particle structures had an equivalent diameter between 200  $\mu\text{m}$  and 400  $\mu\text{m}$ . The particle structures resuspend between a channel length of 51–121 mm. They are accelerated until they reach their maximum velocity and are deposited again at the end of the channel. The achieved maximum velocities of the resuspended particle structures are between 7.2  $\text{ms}^{-1}$  and 10.5  $\text{ms}^{-1}$ . The particle structures are resuspended in the middle of the channel width and remain in the core flow during their transport through the inlet channel of the filter.

Increasing the regeneration temperature from 480 °C to 600 °C and a thin soot layer, the regeneration time is reduced by up to 55% due to the faster oxidation of the soot particles. During the layer break-up, small particle structures are formed. The number of resuspensions increases with the increase of regeneration temperature.

With increasing layer thickness, larger particle structures are formed during layer break-up, and the particle layer breaks-up later. In addition, resuspension starts earlier, the resuspension location shifts towards the end of the channel, and the resuspension time and the number of resuspensions increase. The reduction of the particle layer is comparable for the three layer thicknesses investigated. Increasing the flow rate of the regeneration gas has no influence on the visual layer break-up, but occurs later with increasing flow rate. The number of resuspensions increases with a higher flow velocity, reducing the particle layer more quickly. In further investigations, the particle layer is mixed with ash particles generated by nebulizing engine oil and a subsequent thermal conversion. An internal combustion aerosol with defined properties is to be simulated on a laboratory scale. In this case, the complete inlet channel of the model filter channel will be tracked, and the layer break-up, resuspension, and transport will be analyzed in comparison with the results shown here.

**Supplementary Information** The online version contains supplementary material available at <https://doi.org/10.1007/s40825-023-00228-x>.

**Author Contributions** Conceptualization: J.R.D.T.; methodology: J.R.D.T.; validation: J.R.D.T., H.W., J.M. and A.D.; investigation: J.R.D.T. and H.W.; writing—original draft preparation: J.R.D.T.; writing—review and editing, J.R.D.T., J.M. and A.D.; visualization: J.R.D.T. and H.W.; supervision: J.M. and A.D.; project administration: A.D.

**Funding** We gratefully acknowledge that this project was funded by the Deutsche Forschungsgemeinschaft (DFG, German Research Foundation)-438308378. Open Access funding enabled and organized by Projekt DEAL.

**Data Availability** Not applicable

## Compliance with Ethical Standards

**Ethical Approval** Not applicable

**Conflict of interest** The authors declare that they have no competing interests.

**Open Access** This article is licensed under a Creative Commons Attribution 4.0 International License, which permits use, sharing, adaptation, distribution and reproduction in any medium or format, as long as you give appropriate credit to the original author(s) and the source, provide a link to the Creative Commons licence, and indicate if changes were made. The images or other third party material in this article are included in the article's Creative Commons licence, unless indicated otherwise in a credit line to the material. If material is not included in the article's Creative Commons licence and your intended use is not permitted by statutory regulation or exceeds the permitted use, you will need to obtain permission directly from the copyright holder. To view a copy of this licence, visit <http://creativecommons.org/licenses/by/4.0/>.

## References

- Dittler, A.: The application of diesel particle filters - from past to present and beyond. *Top. Catal.* **60**(3–5), 342 (2017). <https://doi.org/10.1007/s11244-016-0621-z>
- Hanamura, K., Karin, P., Cui, L., Rubio, P., Tsuruta, T., Tanaka, T., Suzuki, T.: Micro- and macroscopic visualization of particulate matter trapping and regeneration processes in wall-flow diesel particulate filters. *Int. J. Engine Res.* **10**(5), 305 (2009). <https://doi.org/10.1243/14680874JER04209>
- Choi, S., Oh, K.C., Lee, C.B.: The effects of filter porosity and flow conditions on soot deposition/oxidation and pressure drop in particulate filters. *Energy.* **77**, 327 (2014). <https://doi.org/10.1016/j.energy.2014.08.049>
- Ishizawa, T., Yamane, H., Satoh, H., Sekiguchi, K., Arai, M., Yoshimoto, N., Inoue, T.: Investigation into ash loading and its relationship to DPF regeneration method. *SAE Int. J. Commer. Veh.* **2**(2), 164 (2009). <https://doi.org/10.4271/2009-01-2882>
- Sappok, A., Wang, Y., Wang, R.Q., Kamp, C., Wong, V.: Theoretical and experimental analysis of ash accumulation and mobility in ceramic exhaust particulate filters and potential for improved ash management. *SAE Int. J. Fuels Lubr.* **7**(2), 511 (2014). <https://doi.org/10.4271/2014-01-1517>
- Okii, H., Karin, P., Hanamura, K.: Visualization of oxidation of soot nanoparticles trapped on a diesel particulate membrane filter. *SAE Int. J. Engines.* **4**(1), 515 (2011). <https://doi.org/10.4271/2011-01-0602>
- Toops, T.J., Pihl, J.A., Finney, C.E.A., Gregor, J., Billeux, H.: Progression of soot cake layer properties during the systematic regeneration of diesel particulate filters measured with neutron tomography. *Emiss. Control Sci. Technol.* **1**(1), 24 (2015). <https://doi.org/10.1007/s40825-014-0008-1>
- Tandon, P., Heibel, A., Whitmore, J., Kekre, N., Chithrapagada, K.: Measurement and prediction of filtration efficiency evolution of soot loaded diesel particulate filters. *Chem. Eng. Sci.* **65**(16), 4751 (2010). <https://doi.org/10.1016/j.ces.2010.05.020>
- Seher, S.I., Ess, M.N., Bladt, H., Niessner, R., Eigenberger, G., Nieken, U.: A comparison of diesel soot oxidation rates measured

- with two different isothermal set-ups. *J. Aerosol Sci.* **91**, 94 (2016). <https://doi.org/10.1016/j.jaerosci.2015.10.003>
10. Sappok, A., Govani, I., Kamp, C., Wang, Y., Wong, V.: In-situ optical analysis of ash formation and transport in diesel particulate filters during active and passive DPF regeneration processes. *SAE Int. J. Fuels Lubr.* **6**(2), 336 (2013). <https://doi.org/10.4271/2013-01-0519>
  11. Kamp, C.J., Sappok, A., Wang, Y., Bryk, W., Rubin, A., Wong, V.: Direct measurements of soot/ash affinity in the diesel particulate filter by atomic force microscopy and implications for ash accumulation and DPF degradation. *SAE Int. J. Fuels Lubr.* **7**(1), 307 (2014). <https://doi.org/10.4271/2014-01-1486>
  12. Schmidt, E., Nitschke, D.: Aufwirbelung von auf Oberflächen abgelagerten Partikelschichten. *Chem Ing. Tech.* **78**(5), 525 (2006). <https://doi.org/10.1002/cite.200600006>
  13. Dittler, A.: Ash transport in diesel particle filters. In: SAE Technical Paper Series. (SAE International400 Commonwealth Drive, Warrendale, PA, United States). SAE Technical Paper Series, (2012). <https://doi.org/10.4271/2012-01-1732>
  14. Hagen, F., Hardock, F., Koch, S., Sebbar, N., Bockhorn, H., Loukou, A., Kubach, H., Suntz, R., Trimis, D., Koch, T.: Why soot is not alike soot: a molecular/nanostructural approach to low temperature soot oxidation. *Flow Turbul. Combust.* **106**(2), 295 (2021). <https://doi.org/10.1007/s10494-020-00205-2>
  15. Dittler, A.: Abgasnachbehandlung mit Partikelfiltersystemen in Nutzfahrzeugen: Zugl.: Wuppertal, Univ., Habil.-Schr., 2014. Wuppertaler Reihe zur Umweltsicherheit (Shaker, Aachen, 2014)
  16. Konstandopoulos, A.G., Skaperdas, E., Warren, J., Allansson, R.: Optimized filter design and selection criteria for continuously regenerating diesel particulate traps. In: SAE Technical Paper Series. (SAE International400 Commonwealth Drive, Warrendale, PA, United States), SAE Technical Paper Series. (1999). <https://doi.org/10.4271/1999-01-0468>
  17. Thieringer, J.R.D., Hafen, N., Meyer, J., Krause, M.J., Dittler, A.: Investigation of the rearrangement of reactive–inert particulate structures in a single channel of a wall-flow filter. *Separations.* **9**(8), 195 (2022). <https://doi.org/10.3390/separations9080195> . <https://www.mdpi.com/2297-8739/9/8/195>
  18. Choi, S., Lee, K.: Detailed investigation of soot deposition and oxidation characteristics in a diesel particulate filter using optical visualization. In: SAE Technical Paper Series (SAE International400 Commonwealth Drive, Warrendale, PA, United States). SAE Technical Paper Series. (2013). <https://doi.org/10.4271/2013-01-0528>
  19. Lapuerta, M., Oliva, F., Agudelo, J.R., Boehman, A.L.: Effect of fuel on the soot nanostructure and consequences on loading and regeneration of diesel particulate filters. *Combust. Flame.* **159**(2), 844 (2012). <https://doi.org/10.1016/j.combustflame.2011.09.003>
  20. Wang, H.C.: Effects of Inceptive motion on particle detachment from surfaces. *Aerosol Sci. Technol.* **13**(3), 386 (1990). <https://doi.org/10.1080/02786829008959453>
  21. Nitschke, D., Schmidt, E.: A new approach to model the re-entrainment of settled particles based on film theory of fluid mass transfer processes. *Part. Part. Syst. Charact.* **26**(1–2), 58 (2009). <https://doi.org/10.1002/ppsc.200800008>
  22. Basu, S., Henrichsen, M., Tandon, P., He, S., Heibel, A.: Filtration efficiency and pressure drop performance of ceramic partial wall flow diesel particulate filters. *SAE Int. J. Fuels Lubr.* **6**(3), 877 (2013). <https://doi.org/10.4271/2013-01-9072>
  23. Zhang, J., Li, Y., Wong, V.W., Shuai, S., Qi, J., Wang, G., Liu, F., Hua, L.: Experimental study of lubricant-derived ash effects on diesel particulate filter performance. *Int. J. Engine Res.* **22**(3), 921 (2021). <https://doi.org/10.1177/1468087419874577>

**Publisher's Note** Springer Nature remains neutral with regard to jurisdictional claims in published maps and institutional affiliations.